PCCP

Accepted Manuscript

ROYAL SOCIETY OF CHEMISTRY

www.rsc.org/pccp

Thermodynamic and Kinetic Studies of $LiNi_{0.5}Co_{0.2}Mn_{0.3}O_2$ as a Positive Electrode Material for Li-ion Batteries using First Principles

*Mudit Dixit, Monica Kosa, Onit Srur Lavi, Boris Markovsky, Doron Aurbach, and Dan Thomas Major**

Department of Chemistry and the Lise Meitner-Minerva Center of Computational Quantum Chemistry, Bar-Ilan University, Ramat-Gan 52900, Israel

*majort@biu.ac.il

ABSTRACT

Ni-rich Li-based layered Ni, Co, and Mn (NCM) materials have shown tremendous promise in recent years as positive electrode materials for Li-ion batteries. This is evident as companies developing batteries for electrical vehicles are currently commercializing these materials. Despite the considerable research performed on $LiNi_{\alpha}Co_{\beta}Mn_{\gamma}O_2$ systems, we do not yet have a complete atomic level understanding of these materials. In this work we study the cationic ordering, thermodynamics, and diffusion kinetics of $LiNi_{0.5}Co_{0.2}Mn_{0.3}O_2$ (NCM-523). Initially, we show that cationic ordering can be predicted employing cheap atomistic simulations, instead of using expensive first-principles methods. Subsequently, we investigate the electrochemical, thermodynamic and kinetic properties of NCM-523 using density functional theory (DFT). Our results demonstrate the importance of including dispersion corrections to standard first principles functionals in order to correctly predict the lattice parameters of layered cathode materials. We also demonstrate that a careful choice of computational protocol is essential to reproduce the experimental intercalation potential trends observed in the $LiNi_{0.5}Co_{0.2}Mn_{0.3}O_2$ electrodes. Analysis of the electronic structure confirms an active role of Ni in the electrochemical redox process. Moreover, we confirm the experimental finding that on complete delithiation, this material remains in an O3 phase, unlike $LiCoO_2$ and NCM-333. Finally, we study various pathways for the Li-ion diffusion in NCM-523, and pinpoint the preferred diffusion channel based on first principles simulations. Interestingly, we observe that the Li diffusion barrier in NCM-523 is lower than that in $LiCoO_2$.

Introduction

Climatic changes, such as global warming, diminishing fossil-fuel reservoirs, and increasing global demands for energy have led to a surge in research on clean and efficient energy storage materials. Rechargeable batteries have shown tremendous promise as alternative energy storage devices, which are based on fundamental electrochemical principles. Within this family of energy storage materials, Li-ion batteries (LIB) have shown superb performance and energy density. Currently, the applications of LIBs extend from small, portable devices such as cell phones to electric vehicles (EVs).[1-6]

$LiCoO_2$ is currently the most widely used positive electrode material in most commercial rechargeable LIBs. This layered material was first reported by Goodenough in 1980,[7] and has been studied extensively since,[8-11] resulting in its commercialization in the early 1990s as a cathode material. Currently, $LiCoO_2$ is used in batteries for most mobile devices. Due to the demand for higher specific energy, many other materials are being investigated, such as the olivine material lithium iron phosphate ($LiFePO_4$)[12] and other olivine phosphates, including $LiCoPO_4$,[13] $LiMnPO_4$[14]and $LiNiPO_4$,[15] and mixed olivines.[16-18] In the quest for high energy density materials for EV applications, materials such as $LiCoO_2$[9] are particularly attractive due to their high theoretical capacity (270 mAh/g).[19] In comparison, $LiFePO_4$ has a much lower theoretical capacity (170 mAh/g)[20]. Unfortunately, in practice, the effective capacity of $LiCoO_2$ is low (148 mAh/g),[21] and combined with safety issues, capacity fading over 4.3V, poor rate performance, and the toxicity of cobalt,[1, 22, 23] this material has limited large-scale applicability.

Motivated by these limitations Ni-rich layered compounds such as $LiNiO_2$[19, 24], $LiNi_{1-\alpha}Co_{\alpha}O_2$,[25] $LiNi_{(1-\alpha)}Mn_{\alpha}O_2$,[26] and $LiNi_{\alpha}Mn_{\alpha}Co_{(1-2\alpha)}O_2$[27, 28] have been proposed and shown to provide superior performance compared to $LiCoO_2$. Many studies have focused on

$LiNi_{0.5}Mn_{0.5}O_2$ and $LiNi_{0.5}Co_{0.2}Mn_{0.3}O_2$ as cathode materials for LIBs.[29-34] Some of these compounds exhibit very high specific capacities (~220 mAh/g), with almost 80% reversible Li de-intercalation.[23] However, in spite of the successful incorporation of Ni-ions into layered materials, Ni-rich materials show significant Ni/Li cation mixing (site exchange). Such cation mixing can lead to capacity fading and structural changes.[35]

A particularly well-studied Li-based Ni, Co, and Mn (NCM) material is $LiNi_{1/3}Co_{1/3}Mn_{1/3}O_2$ (NCM-333), which has a reversible capacity of ~150 mA h/g in an optimal voltage range (~3.5-4.2V).[28] Improvements in electrochemical properties of NCM-333 on reduced graphene oxide coating have recently been demonstrated,[36] and as well as the effect of copper impurities.[37] Koyama et al.[38] studied NCM-333 using density functional theory (DFT) within the local spin density approximation (LSDA), and their calculations suggested that the formal oxidation states of Ni, Co, and Mn in the pristine material are +2, +3, and +4. These authors showed that the energetically favorable structure possesses a so-called $\sqrt{3}\times\sqrt{3}$ R30°-type cation ordering. Furthermore, they also predicted that the redox reactions take place in distinct regions of delithiation space of $Li_xNi_{1/3}Co_{1/3}Mn_{1/3}O_2$ (Ni^{2+}/Ni^{3+} for $0\leq x\leq 1/3$, Ni^{3+}/Ni^{4+} for $1/3\leq x\leq 2/3$ and Co^{3+}/Co^{4+} for $2/3\leq x\leq 1$). DFT calculations using a generalized gradient approximation (GGA) functional, in conjunction with experimental X-ray absorption spectroscopy, supported these findings and identified the valence states of Ni, Co and Mn.[39] Additional studies have also shown that Ni^{+2} is the primary charge compensation site, oxidizing at the lowest potentials.[40, 41] Grey and coworkers have shown that the oxidation state of Ni largely depends on the Li/transition metal (TM) ratio of the starting materials.[42] They have also shown that NCM-333 has a tendency to generate Ni^{+2}-Mn^{+4} cationic clusters, while the Co^{3+} ions adopt random positions.[42] It was also shown that cationic ordering of the material depends on the synthetic procedure and that low short-range and long-range ordering reduces the reversible capacity.[39, 43, 44]

In this work, we study various TM ordering patterns, redox properties, thermodynamics, and lithium diffusion in O3-type NCM-523 using first principles calculations. We present a systematic and funneled approach to predict the cationic TM ordering, which is essential to the electrochemical redox properties of NCMs. This approach is based on initial screening of multiple cationic orderings using classical simulations methods, followed by more accurate DFT scoring. We show that the relative stability of layered materials with different cationic orderings can be well predicted using classical simulation methods, and that the electrochemical, thermodynamic and kinetic properties are nicely described by GGA DFT methods augmented by dispersion corrections. We further demonstrate the possibility of forming solid solutions in partially delithiated states and finally we give extensive atomic and electronic level insight into the workings of NCM-523.

Computational Methods

All atomistic classical calculations were performed using the GULP code.[45] The Buckingham potentials were used to model non-bonded interactions. The Vienna ab-initio simulation package[46-49] (VASP) was used to perform DFT calculations, and these calculations employed the GGA and GGA+U functionals.[50] Specifically, we employed the PBE[51] exchange-correlation functional. Two sets of U values were taken from previous studies[12, 13] on similar classes of materials. In particular, for Ni, Co and Mn, we employed values of U = 5.96, 5.10 and 5.00 eV and U' = 6.40, 3.30 and 3.40 eV, respectively. Spin-polarized DFT with antiferromagnetic spin ordering,[35, 39, 52] was used to relax all structures. The kinetic energy cutoff was chosen to be 520 eV. Due to the very large super-cell, the calculations were performed using the Monkhorst Pack scheme with a mesh of 2×2×1 k-points. To incorporate the effect of dispersion, we employed DFT+D3 method and optPBE-vdW, as implemented in the VASP code.[53-55] Li diffusion barriers were calculated using the nudged elastic band (NEB)[56] method in the fully intercalated limit with gamma k-point only, and a 400 eV kinetic energy cutoff was used. NEB calculations were carried out with the standard PBE functional (without U) to avoid mixing of the diffusion barrier with a charge transfer barrier.[57] The lattice parameters for defect structures were fixed at the relaxed lattice parameters obtained by the PBE+U calculations. Further details of the computational methods are given in the Supporting Information.

Results and Discussion

Cation Ordering:

Mixed TM layered oxides of the NCM family are attractive cathode materials for Lithium-ion batteries. However, NCMs likely have a complex in-plane TM ordering due to the different charges associated with each ion, and it is challenging to get the detailed position of the different ions within the transition metal layer from powder XRD or NMR.[58] This structural uncertainty presents a considerable challenge in first-principles theoretical studies of NCMs, as atomic level resolution of the ionic positions is needed to model these systems and to be able to draw meaningful conclusions.

Previous experimental and theoretical studies have suggested that the transition metals adopt specific cationic ordering patterns, due to the different formal charges associated with the various metal ions.[43] Interestingly, these ordering patterns are governed by simple electrostatic interactions as demonstrated by Cahill et al., using high resolution solid-state ^{6}Li NMR, powder X-ray and neutron diffraction studies.[43] Indeed, these authors suggested that short range cation ordering can be explained using simple electro-neutrality arguments. Grey et al. have shown that layered mixed TM oxides, such as NCM-333, display a (√3x√3)R30 type of ordering (in Wood's notation) within the transition metal layer.[42] A (√3x√3)R30 type of ordering is shown in Fig. 1b. The hexagon in the figure shows that in the (√3x√3)R30 cationic ordering, each type of cation is surrounded by triplets of other types of cations in an alternating fashion.

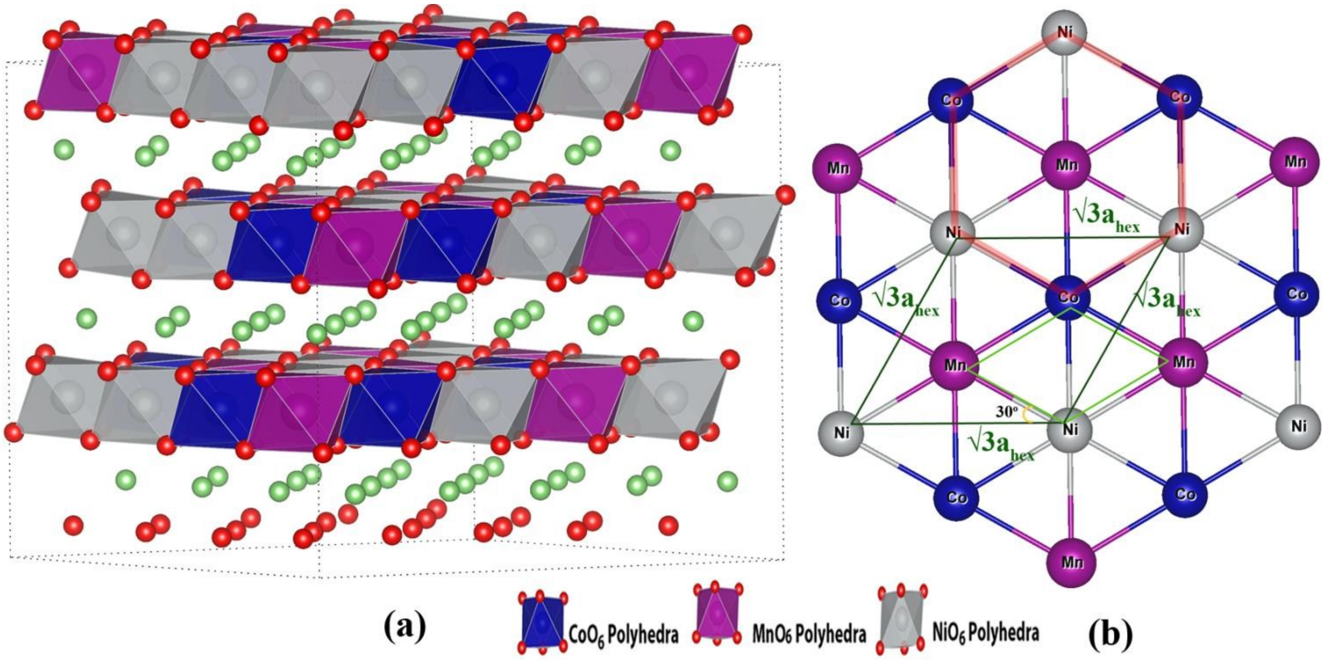

Figure 1. (a) The supercell of NCM-523, Li atoms in green. (b) The (√3×√3) R30 ordering in NCM-333. The dark green colored line shows a √3 ordering.

Weill et al. studied the cationic ordering of $LiNi_{0.425}Co_{0.425}Mn_{0.15}O_2$ using electron diffraction experiments and they confirmed the existence of a $\sqrt{3}a_{hex}\times\sqrt{3}a_{hex}$ superstructure.[59] Meng et al. studied cation ordering in layered O3 $LiNi_xLi_{1/3-2x/3}Mn_{2/3-x/3}O_2$ materials using electron diffraction and powder XRD method, and these authors also found $\sqrt{3}a_{hex}\times\sqrt{3}a_{hex}$ superstructures in all samples.[60] Additional studies have also shown a $\sqrt{3}$x$\sqrt{3}$ R30 type ordering in various layered cathode materials.[61-63]

To elucidate the correct electronic structure and electrochemical properties, such as redox states, voltages and phase stability, of NCM-523 cathode materials, the thermodynamically most stable cationic orderings are required. Presently, to investigate the possible cationic ordering in lithiated NCM-523, we considered three types of in-plane TM orderings, namely linear, random and $\sqrt{3}$-based ordering parameters for Co and Mn (Fig. 2).[35, 42] Initially, we performed antiferromagnetic DFT calculations with several different linear, random and $\sqrt{3}$-based transition metal arrangements. These preliminary calculations clearly suggested that structures with $\sqrt{3}$-type ordering parameters are considerably more stable than structures with other types of arrangements, in agreement with earlier findings.[35, 42]

To rigorously screen all viable structures, we generated all possible $\sqrt{3}$-arrangements for Co and Mn (256 structures for our system setup), using an in-house code. In principle, all these structures could be scored using DFT calculations. However, such calculations are prohibitively expensive, due to the size of the in-silico systems (60 formula units, for a total of 240 atoms). Therefore, we adopted a funneled approach, wherein all structures were initially scored employing a classical force-field (see Methods and Supporting Information). On the basis of these atomistic calculations, we choose the 24 most stable $\sqrt{3}$-structures for further consideration at the DFT level. In Fig. 2 we show the correlation between the DFT and force-field energies for the $\sqrt{3}$-structures, as well as selected linear and random arrangements.

Inspection of Fig. 2 suggests that supercell structures with $\sqrt{3}$-type ordering parameters are more stable than linear and random arrangements, and are also close in energy (0.04-1.62 eV).

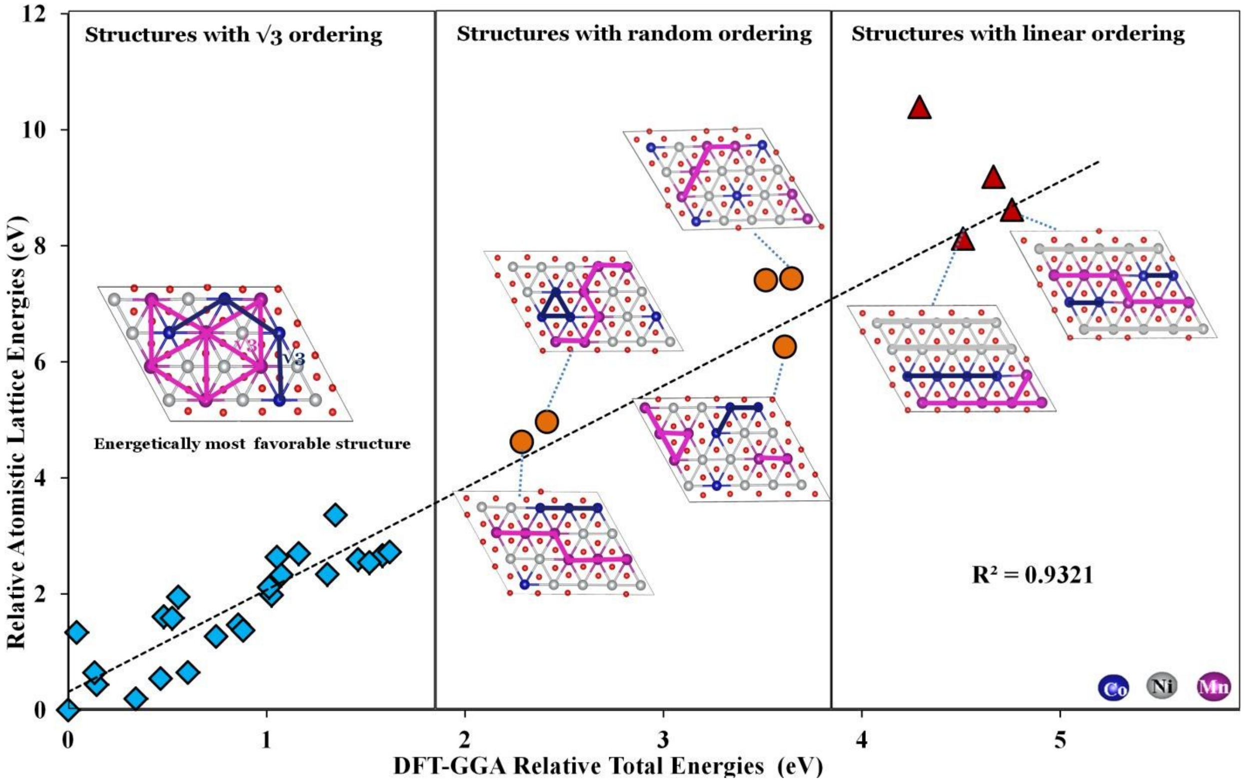

Figure 2. The relative energies (eV) of NCM-523 structures with different ordering parameters using a classical forcefield and the PBE method. Only one transition metal layer is shown for the sake of clarity, although the calculations were performed on the full 60 formula units systems and all the calculations are performed on bulk cathode material only.

The most stable structure shows large Ni-Mn clustering and long range Ni ordering. Interestingly, Grey et al. also found significant Ni-Mn clustering for Ni/Mn-rich NCM samples.[42] Thus, there is good agreement between the general features of the most stable structures computed using our systematic approach and that of previously reported experimental data on other NCM materials.

Structure

The most stable structure found in the previous section was fully relaxed at the various Li-compositions, and multiple Li arrangements were considered for every composition. In the most stable structures, the Li ions were found to be ordered with large Li-Li separations, resulting in minimum interlayer electrostatic repulsion. The relaxed structure of the most stable cationic ordering is shown in Fig. 2, and the accompanying lattice parameters are shown in Table 1. The calculated lattice parameters of lithiated NCM-523 are in good agreement with the experimental lattice parameters,[32] albeit with a slight overestimation, as is typically the case with PBE and PBE+U functionals.[64] For instance, the lattice parameters predicted by PBE for the completely lithiated state (a=2.89Å,c=14.29Å) are in good accord with the corresponding experimental values. However, the best agreement with experiment is obtained when including dispersion. This is particularly true for the c direction, indicating that dispersion is important for the correct description of interlayer interactions.

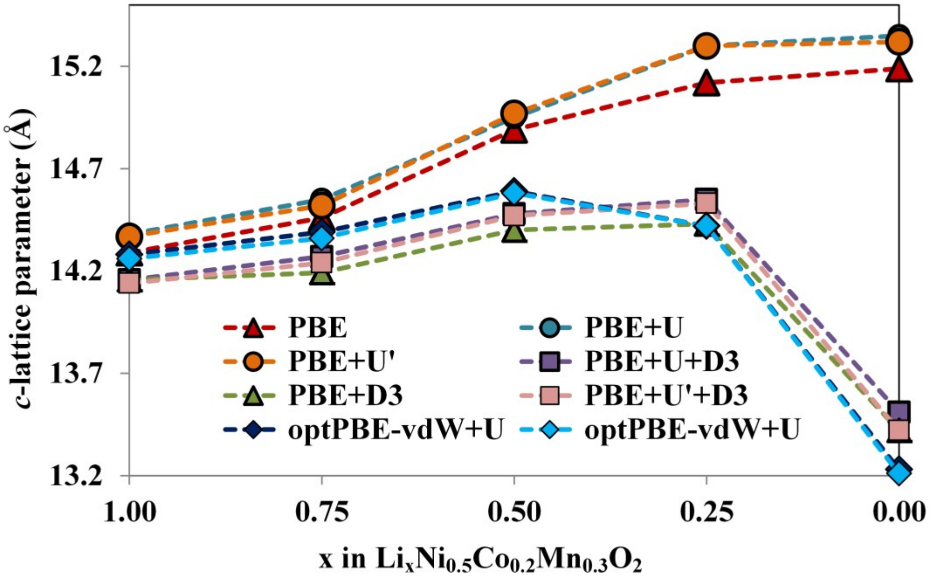

Figure 3. The *c* lattice parameter (Å) of $Li_xNi_{0.5}Co_{0.2}Mn_{0.3}O_2$ at different Li-intercalation levels.

	a	*c*	*a*	*c*	*c*	*c*	*a*	*c*	*a*	*c*
	PBE+U		PBE		PBE+U+D3		optPBE-vdW+U		Exp. [a]	
x=1.00	2.89	14.38	2.89	14.29	2.86	14.16	2.87	14.28	2.86	14.21
x=0.75	2.86	14.55	2.87	14.46	2.84	14.27	2.85	14.39		
x=0.50	2.84	14.99	2.85	14.89	2.81	14.48	2.83	14.59		
X=0.25	2.83	15.30	2.83	15.12	2.80	14.54	2.81	14.42		
x=0.00	2.83	15.35	2.84	15.19	2.81	13.47	2.82	13.23		

[a] Experimental data from Ref. [32].

Table 1. The calculated *a* and *c* lattice parameters (Å) for $Li_xNi_{0.5}Co_{0.2}Mn_{0.3}O_2$ at different Li-intercalation levels.

To appreciate the stability of any cathode material, it is important to understand the changes in lattice parameters on Li extraction. Inspection of Table 1 reveals that there is little change in the lattice parameter *a* upon delithiation of $Li_xNi_{0.5}Co_{0.2}Mn_{0.3}O_2$. This may be ascribed to the fact that largely chemical covalent bonds are aligned along the *a* direction. Specifically, the slight reduction in *a* is due to changes in electrostatic interactions upon Li extraction and changes in the oxidation states of transition metals on de-intercalation. In contrast, the *c* lattice parameter shows considerable variation as a function of lithium content (Fig. 3), and this will be discussed below.

To better understand the somewhat complex behavior for this lattice parameter, it may be instructive to first consider the simpler material, $LiCoO_2$, for which considerable experimental and computational data is available. Experimentally, for $LiCoO_2$, the *c* lattice parameter initially increases as the number of O-Li-O contacts decreases and repulsion between the metal oxide layers increases.[65] Subsequently, at the last stage of delithiation (from x=0.25 to x=0.00), the *c* lattice parameter decreases and this has been ascribed to reduced repulsion between the metal oxide layers, and because of greater electron transfer from oxygen to the oxidized TM layer.[65, 66] This experimentally observed trend is not reproduced employing standard PBE and PBE+U methods,[67] which predict a continuous increase in the *c* lattice parameter, and this may be ascribed to a lack of dispersion in these functionals. Similar monotonous trends for changes in the lattice parameters for $LiCoO_2$ were obtained previously, where PBE overestimates the lattice parameters at the last stage of de-lithiation.[67] We note that the LDA method reproduces the experimental trends in the changes in lattice parameters.[67] Using LDA, Koyama et al. obtained lattice parameter trends in agreement with experiment for $LiCoO_2$, $LiNiO_2$, $LiMnO_2$ and $LiNi_{0.33}Co_{0.33}Mn_{0.33}O_2$,[38, 68] although the *c*-lattice parameters were underestimated. However, these LDA results may be considered somewhat fortuitous, as LDA is known to over-bind at short range,[69] and this functional is not in general expected to outperform GGA methods.

In the current work on NCM-523, the PBE and PBE+U methods predict a continuous increase in the c lattice parameter, similar to that obtained for $LiCoO_2$,[67, 70] and this may be ascribed to a lack of dispersion in these methods.[70] At the last stage of delithiation, with a diluted Li-ion layer, dispersive interactions become important, and hence the PBE and PBE+U methods overestimation *c*. To confirm the role of dispersion interactions in lattice parameter prediction, we applied dispersion corrections to the GGA and GGA+U methods. It is clear from Table 1 that predicted lattice constants using the optPBE-vdW+U (a=2.87Å,c=14.28Å) and PBE+U+D3 (a=2.86Å,c=14.16Å) methods are close to the experimental values (a=2.86Å, c=14.21Å). Importantly, these methods show the expected decrease in the *c* lattice parameter at the last stage of delithiation. This conclusion is in agreement with the recent work of Aykol and Wolverton.[70] Recently, Eames et al. also showed the importance of dispersion corrections in DFT calculations for layered $LiFeSO_4OH$.[71] They showed that the accuracy of voltages for the layered material can only be obtained by including dispersion corrections. As a final point, we mention that experimentally it is known that $LiCoO_2$ and NCM-333 transform from the O3 phase to the O1 phase on complete delithiation.[65, 66] However, NCM-523 does not show this transformation.[31] Our calculations support the O3 phase stability of $LiNi_{0.5}Co_{0.2}Mn_{0.3}O_2$, predicting that the O3 phase is stable by 26 meV/f.u. (formula unit) relative to the O1 phase at the PBE+U+D3 level (22 meV/f.u by PBE).

Electronic Structure

To understand the electrochemical red-ox and phase behavior of NCM-523 during the course of intercalation and de-intercalation, it is necessary to investigate the changes in the electronic structure at different (dis)charging stages.

To understand the redox process during the deintercalation process, we considered Li compositions of x=0.00, 0.25, 0.50, 0.75 and 1.00. In all calculations, we used the most stable structure found with our funneled classical-quantum approach with 60 f.u. Here, we discuss the change in electronic structure using the PBE level of DFT. The total density of states (DOS) and projected DOS (PDOS) at the PBE+U and PBE+U+D3 levels of theory are given in Fig. S1 and S2 of the Supporting Information. We note that the D3 dispersion correction is an empirical correction to the energy and hence changes the geometry of the optimized structure, but not the electronic structure directly.

Figure 4 presents the PDOS of NCM-523 obtained at the PBE level of DFT. For x=1.00, the PDOS of NCM-523 clearly shows that even in the pristine material, Ni exists in two different charge states, corresponding to formal oxidation states of +2 and +3 (Fig. 4b). Inspection of this figure shows that Ni^{+2} and Ni^{+3} have electronic configurations corresponding to $t_{2g}^6e_g^2$ (high-spin) and $t_{2g}^6e_g^1$, respectively (see also Fig. 6). Clearly, the exchange splitting of Ni^{+2} is significantly higher than that of Ni^{+3} due to a higher number of unpaired electrons in Ni^{+2}. The Mn^{+4} corresponds to a $t_{2g}^3e_g^0$ high-spin configuration (see also Fig. 6), while the Co^{+3} ions represent an electronic configuration of $t_{2g}^6e_g^0$. As expected, for Co^{+3} there is no exchange splitting for the electronic states. The valence band maximum (VBM) is formed by Ni^{+2}-e_g and Ni^{+3}-e_g, whereas the conduction band minimum (CBM) primarily consists of Ni^{+3}-e_g states. At x=1.00, both the VBM and CBM consist primarily of Ni states. This strongly suggests that Ni is the most electrochemically active transition metal in NCM-523. Interestingly, similar results were obtained by Ceder et al.[39] for NCM-333. These authors suggested that Ni represents the main charge compensation site, and Ni^{+2} oxidizes at the lowest potentials upon Li-deintercalation. Our results for the local valence states of the metal ions suggest that in NCM-

523 (in the pristine state), 60% of the Ni ions are in a +2 charge state and 40% of the Ni ions are in a +3 charge state. The average oxidation state of Ni is +2.4. Interestingly, our results are somewhat different to that of computational results of Kim et al. for NCM-523, who suggested that Ni is in a pure +2 state.[72] The reason for this discrepancy is likely the more accurate TM-composition employed in the current work. Indeed, Kim et al. considered a relatively small 12 f.u. super cell, corresponding to a Ni:Co:Mn ratio of 6:3:3, in contrast to the current work, which employed a 60 f.u. super cell, facilitating an exact 5:2:3 ratio. We note that to accurately determine the local valence states of different Ni atoms, it is essential to maintain an atomic ratio exactly as in the experiments, and hence it is necessary to employ larger supercells in the calculations.

Kim et al. also suggested that fractional occupancies of *d* states of Ni ions are higher in NCM-523 than in $LiNiO_2$.[72] Based on our calculations, we attribute this to the presence of significant amounts of Ni^{+2} in NCM-523 (60.0%), compared to 0.0% in $LiNiO_2$. Comparing the results for NCM-333,[39] NCM-721[72] and our results for NCM-532, we suggest that the oxidation states of Mn and Co remain invariant in these materials. Indeed, in Ni rich NCMs ($LiNi_{\alpha}Co_{\beta}Mn_{\gamma}O_2$; $\alpha+\beta+\gamma=1$), the change in TM charge distribution as a function of composition may be ascribed largely to changes in the oxidation states of Ni. As Ni acts as the main charge compensation metal, one can speculate that introduction of dopants might enhance the capacity of Ni-rich NCMs due to fine-tuning the amount of Ni^{+2} via charge compensation.

The integrated PDOS (IPDOS) up to the Fermi level (Table S3), supports the deduced electronic structure. The difference in IPDOS between the up and down spins gives a rough estimate of the number of unpaired electrons. The difference in IPDOS for Ni^{+2} (1.33 a.u.) is significantly higher than that of Ni^{+3} (1.15 a.u.). For Co^{+3} this difference is close to zero (0.01 a.u.), while in the case of Mn^{+4} the difference in IPDOS is 3.22 (a.u.).

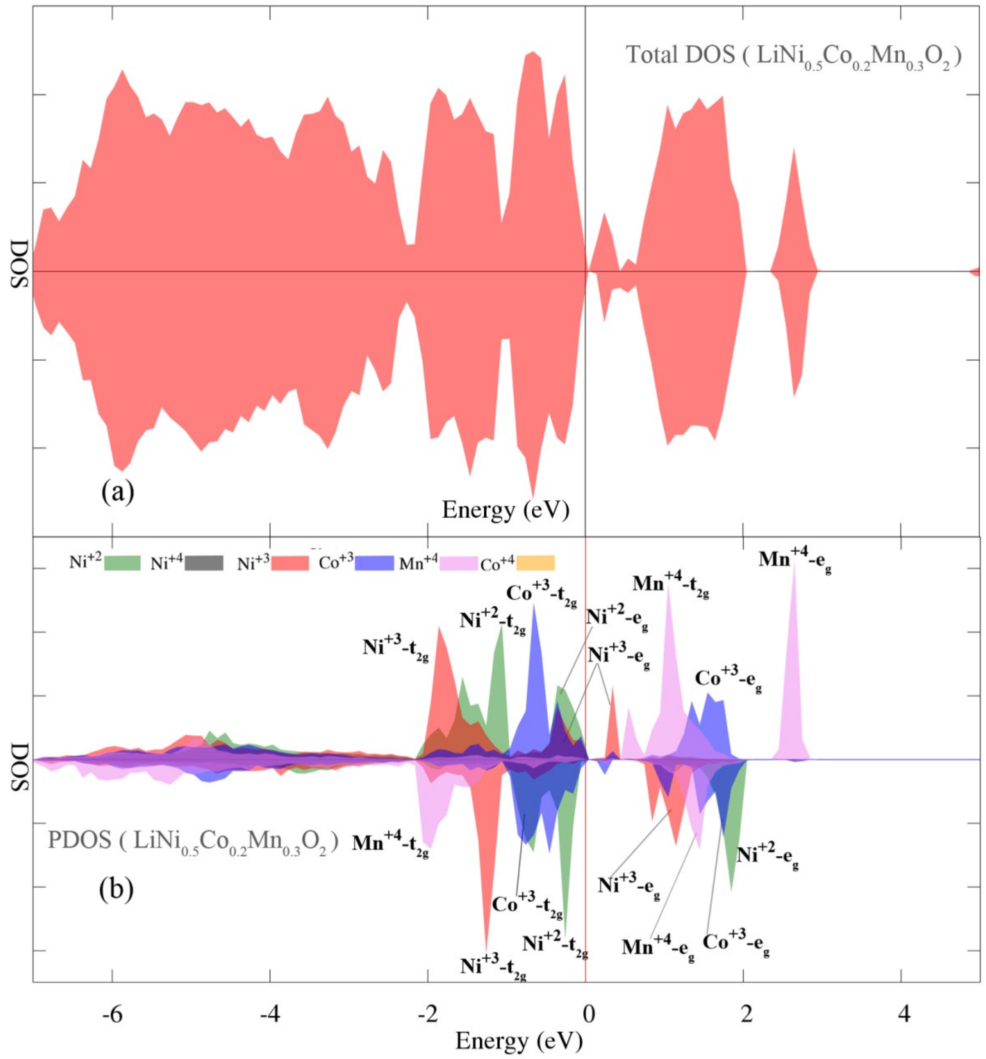

Figure 4. Density of states of $Li_xNi_{0.5}Co_{0.2}Mn_{0.3}O_2$ at x=1.00 (a) total DOS (b) projected DOS using PBE.

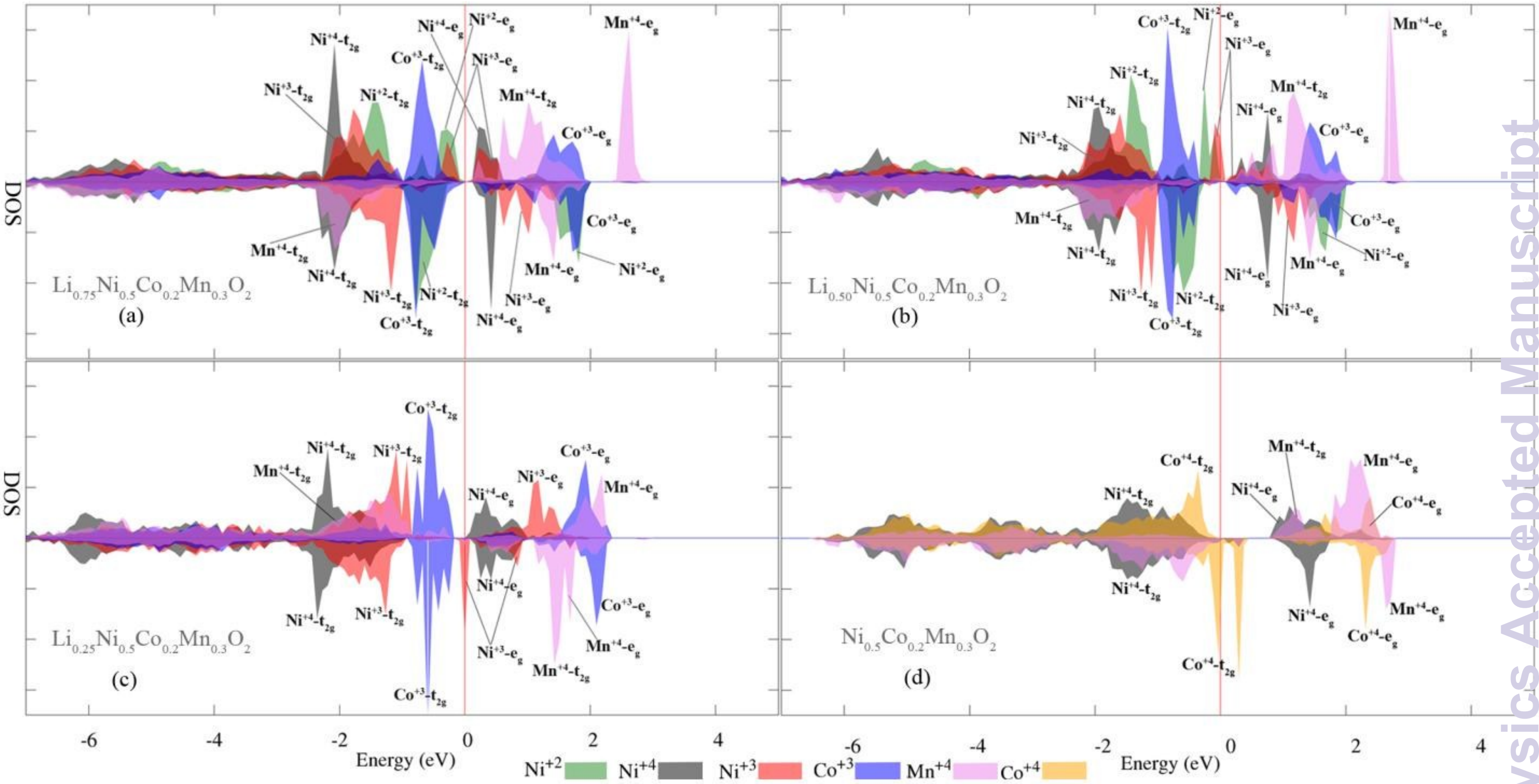

Figure 5. Projected Density of States of $Li_xNi_{0.5}Co_{0.2}Mn_{0.3}O_2$ at (a) x=0.75, (b) x=0.50, (c) x=0.25 and (d) x=0.00 using PBE.

For x=0.75, the PDOS of NCM-523 shows the existence of Ni^{+4}, along with Ni^{+2} and Ni^{+3} (Fig. 5a). The Ni^{+2} has the electronic configuration $t_{2g}^6e_g^2$ (high-spin), Ni^{+3} may be described as $t_{2g}^6e_g^1$, whereas Ni^{+4} as $t_{2g}^6e_g^0$ (Fig. 5a). As expected, there is some exchange splitting for both Ni^{+2} and Ni^{+3}, but not for Ni^{+4}. The occupancies of the Mn and Co states remain the same as for x=1.00. Interestingly, Ni^{+2}-e_g is slightly pushed away from the Fermi level, whereas Ni^{+3}-e_g is pushed towards the Fermi level. At x=0.75, the VBM primarily consists of e_g states of Ni^{+3} and Ni^{+4}, where the CBM consists of Ni^{+2} and Ni^{+3} e_g states. This occupation of frontier states suggests that at a x=0.75 intercalation level, both Ni^{+2} and Ni^{+3} are involved in the electrochemical redox process.

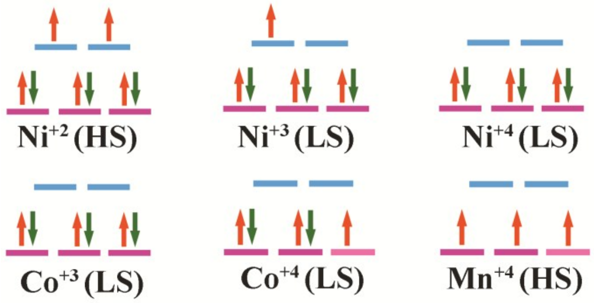

Figure 6. Suggested electronic configuration for the transition metal ions in NCM-523 at different intercalation levels.

The PDOS of NCM-523 clearly shows that at x=0.50 (Fig. 5b), Ni^{+2} has an electron distribution corresponding to $t_{2g}^{6}e_{g}^{2}$ (high-spin), Ni^{+3} has electronic configuration $t_{2g}^{6}e_{g}^{1}$, while Ni^{+4} is $t_{2g}^{6}e_{g}^{0}$. The Mn^{4+} configuration may be described as $t_{2g}^{3}e_{g}^{0}$, while for Co^{+3} the configuration is $t_{2g}^{6}e_{g}^{0}$. The VBM primarily consists of e_g states of Ni^{+3} and Ni^{+4}, whereas the CBM consists of Ni^{+2}- and Ni^{+3}-e_g states. This occupation of frontier states suggests that at a x=0.50 intercalation level, Ni^{+2}, Ni^{+3} and Ni^{+4} are all involved in the electrochemical redox process.

For x=0.25 (Fig. 5c), Ni^{+3}-e_g is further pushed towards the Fermi level, and even crossing it. This suggests that the main redox reaction at this intercalation level is due to the pair Ni^{+3}/Ni^{+4}. Interestingly, Co^{+3}-t_{2g} is also pushed toward the Fermi level. Ni^{+3} is in a $t_{2g}^{6}e_{g}^{1}$ state, whereas Ni^{+4}-t_{2g} is fully occupied ($t_{2g}^{6}e_{g}^{0}$). The occupancies of the Mn^{+4} states remain the same as for x=1.00.

For x=0.00, the Mn^{+4}-t_{2g} orbitals are spin-singly occupied and the Mn^{+4}-e_g orbitals are spin doubly unoccupied (Fig. 5d). The Co^{+3} and Ni^{+3} orbitals have vanished, indicating the complete oxidation of Co^{+3} to Co^{+4} and Ni^{+3} to Ni^{+4}. The Co t_{2g} orbitals show exchange splitting with Co t_{2g} spin-singly unoccupied ($t_{2g}{}^{5}e_g{}^{0}$). The Ni^{+4} t_{2g} orbitals are fully occupied and the Ni-e_g orbitals are fully unoccupied with no exchange splitting ($t_{2g}{}^{6}e_g{}^{0}$). At this intercalation level, the VBM and CBM consist of e_g of Co^{+4} states only.

Electrochemical Redox Behavior

To design new positive electrode materials and optimize the performance of existing ones, it is important to understand the electrochemical redox behavior of these cathodes on Li de-intercalation. By inspecting the magnetic moments (see Fig. S3) and the electronic structure of NCM-523 we found that Ni is present in both +2 and +3 states in the pristine material. Fig. 7 shows the changes in oxidation states on Li de-intercalation using the PBE and PBE+U functional. For x=1.00, the calculated magnetic moments on Ni atoms show that in the fully lithiated unit cell (60 f.u.) 18 out 30 Ni ions are in a formal +2 oxidation state (magnetic moment ~1.7) and 12 Ni ions are in a +3 oxidation state (magnetic moment ~1.1) (Fig. 7). In a very recent study, Wei et al. reported a ratio of Ni^{+2}:Ni^{+3}:Ni^{+4} in pristine Li-NCM 523 of 3:2:0.[33] Our results are in agreement with the reported data. The formal oxidation states of Co and Mn are found to be +3 (magnetic moment ~0.0) and +4 (magnetic moment ~3.2), respectively. On removal of Li to yield x=0.75, Ni^{+2} and Ni^{+3} oxidize to Ni^{+3} and Ni^{+4}, respectively. At this intercalation level, Ni exists in +2, +3 and +4 oxidation states (Fig. 7). The calculated magnetic moments on Ni atoms show that at x=0.75, 5 of 30 Ni ions are in a +2 formal oxidation state (magnetic moment ~1.7), 23 Ni ions are in a +3 oxidation state (magnetic moment ~1.1), while 2 Ni ions are in a +4 oxidation state (magnetic moment ~ 0.0). The noticeable increase in the number of Ni^{+3} and decrease in the number of Ni^{+2} ions during the x=1.00 to 0.75 transformation, suggest that a Ni^{+2}/Ni^{+3} redox reaction is mainly involved in this range. For x=0.50, the calculated magnetic moments on the Ni atoms show that 1 of 30 Ni ions is in a formal +2 oxidation state (magnetic moment ~1.7), 16 Ni ions are in a +3 oxidation state (magnetic moment ~1.1), while 13 Ni ions are in a +4 oxidation state (magnetic moment ~ 0.0). At this stage most of the Ni^{+2} are oxidized to Ni^{+3} or Ni^{+4}. Wei et al. have also reported the ratio of Ni^{+2}:Ni^{+3}:Ni^{+4} to be 0:3:2.[33] A considerable decrease in the number of Ni^{+2} and Ni^{+3} ions suggests that Ni^{+2}/Ni^{+3} and Ni^{+3}/Ni^{+4} redox reactions are occurring in the $0.50 \leq x \leq 0.75$ range. For x=0.25, all Ni^{+2} are oxidized, 3 Ni ions are in a +3 state, and 27 Ni ions are in a +4 oxidation state. The decrease in the number of Ni^{+3} ions suggests that Ni^{+3}/Ni^{+4} constitute the active redox pair for $0.25 \leq x \leq 0.50$. For x=0.00 all transition metals oxidize to a +4 oxidation state. At this intercalation level a Ni^{+3}/Ni^{+4} redox reaction is mainly responsible for the electrochemical activity ($0.00 \leq x \leq 0.25$). We note that inspection of Fig. 5 clearly shows that the DOS at the Fermi level for $Li_xNi_{0.5}Co_{0.2}Mn_{0.3}O_2$ consists solely of Ni and Co states at all intercalation levels, with the former ion making the major contribution. Mn remains fixed in a +4 oxidation state. Therefore, we conclude that Ni is mainly responsible for the electrochemical properties of this material. Using X-ray photo electron spectroscopy Kim et al. have also demonstrated the existence of Ni^{+2}, $Ni^{+3}$and Mn^{+4} in the pristine material.[72]

In Fig. 8 we present the differential capacity plots measured for NCM-523 electrodes at a C/5 rate (30^0C), demonstrating clearly oxidation/reduction waves related to $Ni^{2+} \Leftrightarrow Ni^{3+} \Leftrightarrow Ni^{4+}$ and $Co^{3+} \Leftrightarrow Co^{4+}$ processes in the potential range of 3.7 – 3.8 V and at higher potentials, respectively. These processes accompany the Li-ions extraction/insertion during charge/discharge of NCM-

523 electrodes. This is in agreement with the recent study by Wang et al.[73] We note that the differences in the oxidation and reduction waves seen in Fig. 8 are likely due to more sluggish kinetics of the Ni^{4+}/Ni^{2+} reduction process compared to the oxidation of Ni^{2+}/Ni^{4+}. A possible reason for the more sluggish kinetics of the Ni^{4+}/Ni^{3+}/Ni^{2+} reaction concomitant with the Li^{+} intercalation, can be a complex (and resistive) structure of an interface (SEI) formed. Such an interface may contain Ni^{4+} and Ni^{3+} species, like NiO$_2$, spinel phase Li$_x$Ni$_2$O$_4$, rock-salt Li$_{1-x}$Ni$_x$O and NiF$_4$ from which the reduction reaction is deteriorated due to the increased interfacial impedance.[73]

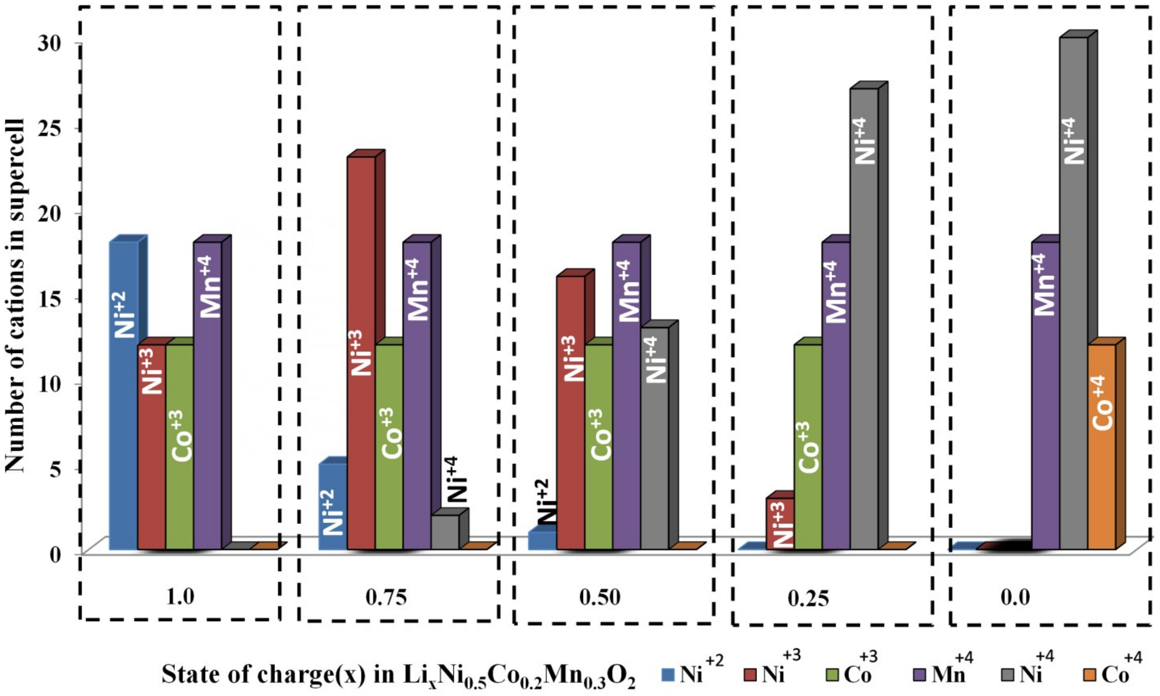

Figure 7. Oxidation states for different transition metals of Li$_x$Ni$_{0.5}$Co$_{0.2}$Mn$_{0.3}$O$_2$ at x=1.00, x=0.75, x=0.50, x=0.25 and x=0.00.

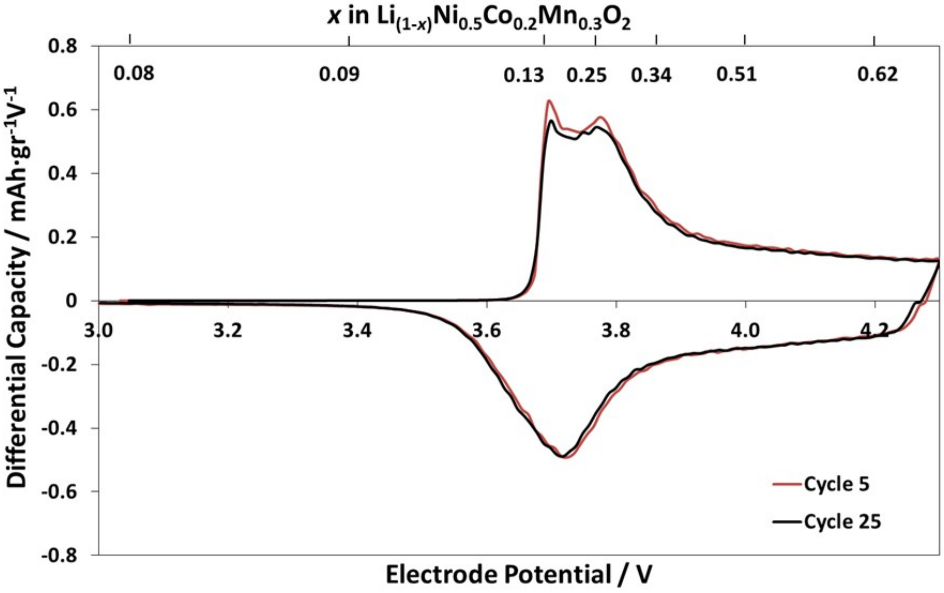

Figure 8. Typical differential capacity plots measured for NCM-523 electrodes cycled at a C/5 rate in a Li-cell with EC-EMC/$LiPF_6$ solution at 30^0C. The top *x*-axis represents the amount of lithium (x in $Li_{1-x}Ni_{0.5}Co_{0.2}Mn_{0.3}O_2$) upon the electrode's charging.

Electrochemical Stability

The structural stability of cathode materials during delithiation is crucial for the application of metal oxides as successful cathode materials. Indeed, structural instability may cause rapid capacity fading. For example, charging $LiCoO_2$ at high voltages results in positive potential shifts at the anode and subsequent oxygen loss with further structural transformations.[22] This issue limits practical reversible capacity of $LiCoO_2$ due the instability of the host structure at higher voltages. For many cathode materials, lower operation potentials are suggested to avoid structural transformation at higher voltages. During the de-intercalation process the oxidation states of transition metals vary. This variation in oxidation states may also cause structural instability, leading to structural transformations at intermediate Li loading. A solid solution with uniform distribution of Li ions at partially de-intercalated states could provide the desired phase-stability upon the dynamical process of delithiation and avoid phase separation into fully intercalated and fully de-intercalated phases. To thermodynamically characterize the structural stability of partially de-intercalated states, Van der Ven et al. defined the formation energy as:[74]

$$E_F = E(Li_xMO_2) - xE(LiMO_2) - (1-x)E(MO_2) \qquad (1)$$

where $E(Li_xMO_2)$ is the total energy (per formula unit) of partially de-intercalated states, $E(LiMO_2)$ is the total energy of fully intercalated states and $E(MO_2)$ is the total energy of fully deintercalated states. Determination of the correct ordering of Li ions and vacancies in the Li layers is very important for computation of accurate formation energies. Therefore, we performed various calculations of Li ordering at different deintercalation levels. The lowest energy structures (i.e. optimal Li ion distribution) were employed for the calculation of the formation energy.

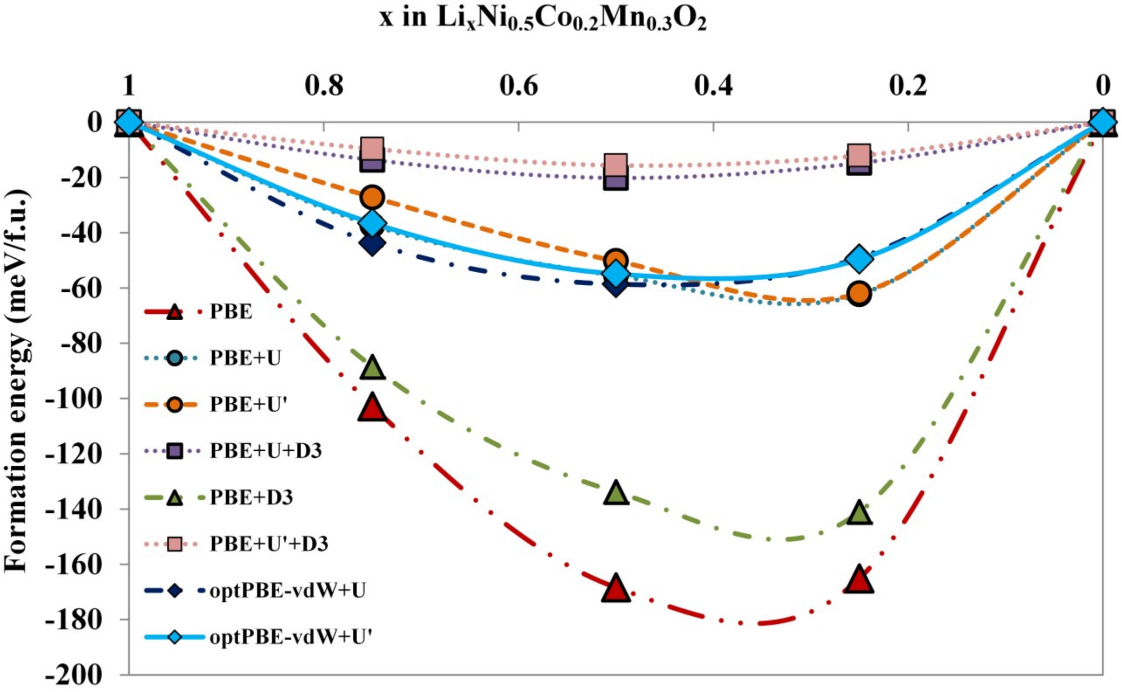

Figure 9. Calculated formation energies of $Li_xNi_{0.5}Co_{0.2}Mn_{0.3}O_2$ at different deintercalation levels.

The formation energy at a particular concentration of Li indicates the relative stability of that structure with respect to the phase-separated species. Negative formation energy suggests that at a given concentration of Li, the system prefers to reside in the solid solution state rather than phase separate into MO_2 and $LiMO_2$. Fig. 9 shows the formation energies of $LiNi_{0.5}Co_{0.2}Mn_{0.3}O_2$. It is clear from Fig. 9 that the formation energies of partially intercalated states are negative for NCM-523, and hence predict a solid solution behavior. We note that all methods employed in this study predict negative formation energies, although the magnitudes of the PBE+U based methods are significantly lower than that of the PBE based methods. The different formation energies obtained with addition of U to the PBE method can be attributed to three possible reasons. Firstly, the electron correlation in A_xCoO_2 (A=Li, Na)-based materials changes as a function of intercalation level.[75-78] Secondly, as a result of varying contribution of electron correlation as a function of alkali-ion content, the Hubbard U-parameter should depend on the intercalation level (i.e. U should depend on the oxidation state of the TMs). However, this would preclude comparing the energies at the different intercalation levels. Lastly, it was shown experimentally[79, 80] and theoretically[81] that in the de-intercalation process of $LixCoO_2$-based systems, delocalized electrons on oxygen atoms play a significant role. However, the PBE+U method artificially localizes electrons on TMs instead of on oxygen atoms. Due to the above reasons we propose that GGA based methods are more appropriate for the calculation of formation energies. It is noteworthy that inclusion of the D3 dispersion correction slightly reduces the absolute value of the formation energy, while inclusion of dispersion in the form of the optPBE-vdW functional has little effect on the computed formation energy.

Average intercalation Voltage

The intercalation reaction of NCMs can be given as:

$$Li(x_1\text{-}x_2)NCM + x_2Li(bulk) \leftrightharpoons Lix_1NCM \qquad (2)$$

The average intercalation voltage depends on the chemical potential of the above reaction. The cell voltage V can be expressed as:[82]

$$V(x) = \frac{\mu_{Li(x)}^{cathode} - \mu_{Li}^{anode}}{F} \qquad (3)$$

where μ_{Li}^{anode} is the chemical potential of the alkali anode, and usually bulk metal is chosen as the anode and F is Faraday's constant. Then the average voltage can calculated as:[83]

$$V = \left\{ \frac{E(Li_{x+dx}NCM) - E(Li_x NCM)}{dx} - E(Li_{bcc}) \right\} \qquad (4)$$

where $E(Li_{x+dx}NCM)$ and $E(Li_x NCM)$ represent the total energy per formula unit of the system before and after lithium de-intercalation. Various vacancy configurations were constructed, and we choose the most stable one for our considerations. We note that the calculations model states at thermodynamic equilibrium and mimic experimental voltage profiles obtained at a slow galvanostatic rate. The intercalation potentials using the PBE and PBE+D3 methods show trends comparable to the experimental results, although the absolute values are consistently underestimated relative to the experimental values (Table 2). Hence, shifted PBE voltages for NCM-523 show very good agreement with the experimental data (Fig. 10),[32] and we note that such shifting is commonly applied.[35] The absolute average voltages using the PBE+U method (Table 2) are in better agreement with the experimental voltages (~4.2 V) than PBE, but PBE+U is less successful in reproducing the fine details in the trends of the experimental voltages (Fig. 10). Dispersion correction in conjunction with U (PBE+U+D3 and PBE+U'+D3) slightly increases the average voltages, while showing only a slight increase in voltages with Li de-intercalation. The PBE+U functional with built-in dispersion (optPBE-vdW+U and optPBE-vdW+U') gives higher voltages compared to PBE+U, but shows similar voltage trends as obtained with the PBE+U method. The relatively poor performance of the PBE+U method in computing voltage profiles in layered NCM can be attributed to the same factors as for the calculation of formation energies: change in electron correlation as a function of intercalation species,[75, 77, 78, 84] dependence of the optimal U on the TM oxidation state, and the artificial localization of electrons on TM centers rather than on oxygen atoms.[81] Singh et al. have recently shown that for weakly correlated systems such as Co_3O_4, the PBE method outperforms PBE+U in the prediction of electronic structure when compared to hybrid functionals like HSE06 and experiments.[85] Recently it was shown that despite the overestimation of average voltages, GGA predicts good voltage trends in $LiCoO_2$ compared to experimental data, and performs as well as hybrid functionals (e.g. HSE06) with optimized mixing parameters, whereas GGA+U fails to predict correct voltage trends.[81] The above discussion suggest that GGA based methods, such as the PBE functional, may be more appropriate for voltage calculations in layered $LiCoO_2$ based systems.

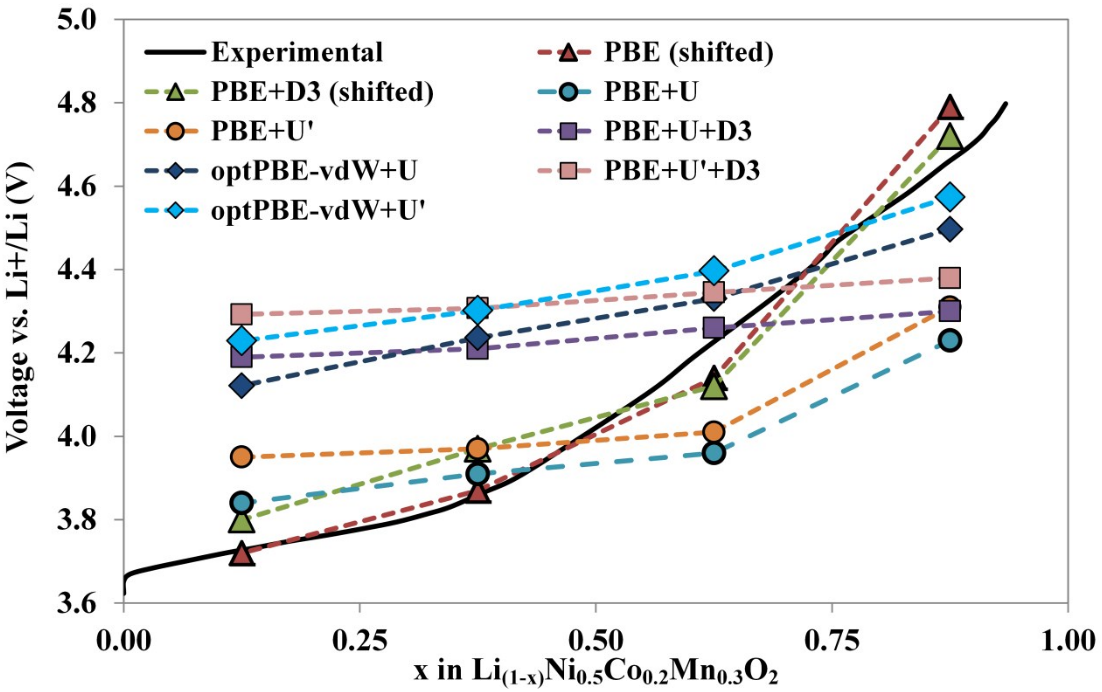

Figure 10. Calculated and experimental intercalation potentials for $Li_xNi_{0.5}Co_{0.2}Mn_{0.3}O_2$ at different delithiation levels. GGA values are shifted[35] by 0.9 eV and GGA+D3 are shifted by 0.6 eV. The black line represents the experimental data from Ref.[33]. The experimental data are plotted by considering a specific capacity of 250 mAh/g in the fully delithiated limit.

Intercalation Range[a]	Average Voltage(V)							
	PBE	PBE+U	PBE+U'	PBE+D3	PBE+U+D3	PBE+U'+D3	optPBE-vdW+U	optPBE-vdW+U'
x=0.0-0.5	3.57	4.10	4.16	3.82	4.28	4.36	4.41	4.48
x=0.5-1.0	2.89	3.87	3.96	3.28	4.20	4.29	4.17	4.26

[a] x in $Li_xNi_{0.5}Co_{0.2}Mn_{0.3}O_2$

Table 2. The calculated average voltages (V) for $Li_xNi_{0.5}Co_{0.2}Mn_{0.3}O_2$ in different Li-intercalation ranges.

Li Diffusion

High Li-ion diffusion rates are key for the power density of the cathode. Usually the power density of LIBs is limited by the cathode component, i.e. by the Li-ion diffusion kinetics. Importantly, the kinetics of ion diffusion can be fine-tuned based on an understanding of the various ion diffusion pathways. For Li-ion batteries, the rate of diffusion along a certain path depends on many factors such as the structure of the host, electrostatic and steric interactions between the ion and the host at the initial and transition states, as well as the number of vacancies.[86] The rate of ion diffusion can be computed within the framework of transition state theory by

$$k = \frac{k_B T}{h} \frac{Q^{TS}}{Q^{IS}} e^{-\beta \Delta E^{\ddagger}} \qquad (5)$$

where h is Plank's constant, $\beta = (k_{\mathrm{B}} T)^{-1}$, k_{B} is Boltzmann's constant and T is the temperature, and Q_{M}^{IS} and Q_{M}^{TS} are the partition functions in the initial state (IS) and the transition state (TS), respectively. The ratios of partition functions can be given as:

$$\frac{Q_{TS}}{Q_{IS}} = \frac{h}{k_B T} \times \frac{\prod_{i}^{3N-6} v_i}{\prod_{i}^{3N-7} v'_i} \qquad (6)$$

where v_i and v'_i are the vibrational frequencies of the IS and the TS, respectively. The diffusion constant can be written as:

$$k = \omega \times e^{-\beta \Delta E^{\ddagger}} \qquad (7)$$

where $W = \frac{\prod_{i}^{3N-6} v_i}{\prod_{i}^{3N-7} v'_i}$ is the hopping frequency, which determines the difference in the entropy of the IS and TS. The hopping frequency has a magnitude in the order of a single phonon frequency. A reasonable approximation for ω is 10^{13} sec^{-1}.[87] Diffusion rate is then given by:

$$\Gamma = l^2 k \tag{8}$$

where l is the concentration coefficient (ion diffusion length).

Li diffusion in layered $LiCoO_2$ was first studied by Van der Ven et al.[87], and they found two distinct Li migration pathways, which they dubbed oxygen dumbbell hop (ODH) and tetrahedral site hop (TSH).

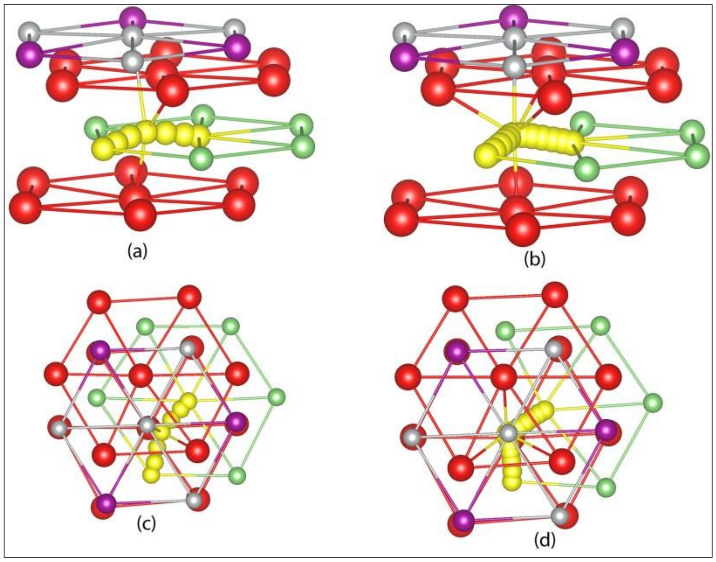

Figure 11. Li diffusion paths for fully lithiated $Li_xNi_{0.5}Co_{0.2}Mn_{0.3}O_2$ (a) ODH path (b) TSH path (c) top view of ODH path (d) top view of TSH path. Color code for spheres: Red – oxygen atoms, green – Li atoms, grey – Ni atoms, pink – Mn atoms. Yellow spheres indicate NEB images for the Li atoms. Only Li migration part of the system is shown for clarity, although the calculations were performed on the full 60 formula units systems.

Figure 11 shows the ODH and TSH diffusion paths of Li in $LiNi_{0.5}Co_{0.2}Mn_{0.3}O_2$. Careful examination of both paths suggests that for a mono vacancy scenario, only the ODH pathway is viable.[87] This is due to electrostatic repulsion between migrating Li ions and occupied site Li ions. Indeed, we observe a short distance (R(Li-Li)=2.4 Å) between the migrating ions and neighboring ions at the TS. However for the divacancy scenario, an additional neighboring Li-site is unoccupied, and hence the migrating atom can pass via both a dumbbell hop and a tetrahedral site.

Three main interactions of the migrating ions at the TS of the ODH pathway are Li-M (with the transition metal, Ni^{+2}, in the transition metal layer), Li-Li' (migrating Li ion feels electrostatic repulsion with a neighboring Li' atom) and Li-O interaction at the dumbbell site with short Li-O distances (1.79 and 1.82 Å). Therefore, due to strong steric hindrance, one would expect a large ion diffusion barrier for Li^+ along the ODH pathway. Our NEB calculations confirm this hypothesis, and indeed we find a barrier of 0.50 eV for Li^+ diffusion along this pathway (Fig. 12a). Van der Ven et al. found a Li^+ diffusion barrier of 0.82 eV for Li diffusion in $LiCoO_2$ along the ODH pathway.[87] In $LiCoO_2$, Co is in a +3 oxidation state, and hence possesses greater electrostatic repulsion with Li^+ than Ni^{+2} (in NCM-523). Additionally, the interlayer distance in NCM-523 is larger than that of $LiCoO_2$, providing a more spacious diffusion pathway than in $LiCoO_2$. Kang et al. have previously shown a linear increase in the diffusion barrier with decreased c lattice parameter values.[88] Indeed, they showed that a 4% decrease in the c lattice parameter increases the Li diffusion barrier by more than 200%.[88, 89] We therefore ascribe the lower diffusion barrier in NCM-523 than in $LiCoO_2$ to a combination of steric and electrostatic effects. Using classical molecular dynamics, Li et al. found a Li diffusion barrier of 0.56-0.63 eV for Li NCM-333.[90] Our results are similar to their findings, in spite of the different material composition. We note that a lower barrier for Na diffusion in NaNCM-333 compared to $NaCoO_2$ has been shown recently.[91]

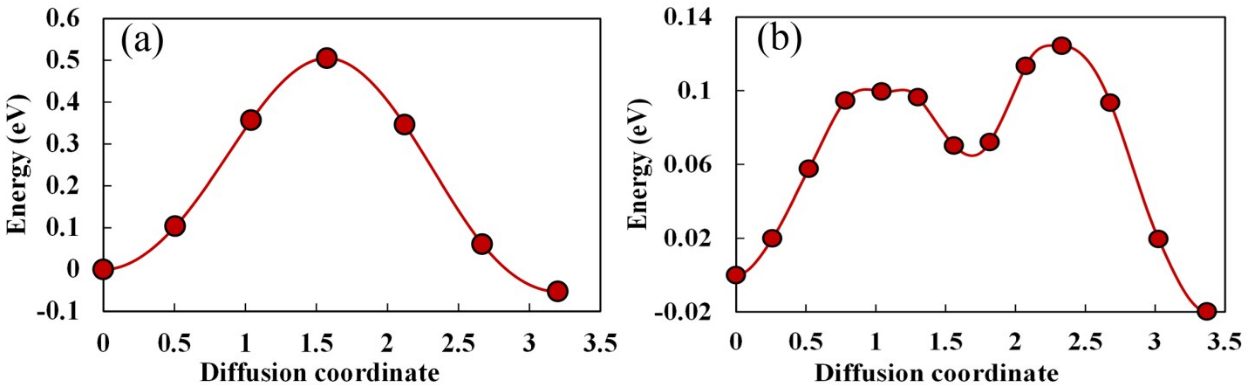

Figure 12. Li diffusion barrier profiles for the (a) ODH path (b) TSH path in $LiNi_{0.5}Co_{0.2}Mn_{0.3}O_2$.

We now turn our attention to the TSH pathway, and note that the main requirement of TSH pathways is the availability of Li di-vacancies to allow Li migration via a tetrahedral intermediate. In the TSH pathway, the interactions between the migrating Li ions and the host matrix are similar than that of ODH pathway, but the presence of a di-vacancy minimizes the repulsion between the migrating Li. Consequently, ions can hop through tetrahedral intermediate sites without passing through sterically constrained oxygen dumbbell sites. This results in a significant lowering of the barrier for the TSH pathway. Ong et al. have recently reported an ion diffusion barrier of 0.21 eV for Li diffusion in $LiCoO_2$ via a TSH diffusion pathway using a 5x5x1 supercell.[57] As speculated, our computed Li diffusion barrier (Fig. 12b) for the TSH pathway (0.12 eV) is found to be lower than that of the ODH pathway. Interestingly, the TSH barrier for NCM-523 is lower than that of $LiCoO_2$ because of the weaker repulsive Li^+-Ni^{+2} interactions at the transition state (compare with Li^+-Co^{+3} in $LiCoO_2$) and a larger *c* lattice parameter of NCM-523. Based on the lower Li diffusion barrier of NCM-523, we suggest that NCM-523 has better rate capabilities compared to $LiCoO_2$. We also note that unlike $LiCoO_2$, the minimum energy diffusion profile for NCM-523 is asymmetrical because of anisotropy in the potential energy surface due the changing environment during Li migration (Li^+-O-Ni^{+2}, Li^+-O-Co^{+3} and Li^+-O-Mn^{+4}). The maxima of the TSH pathway correspond to the NEB images with smallest O-Li-O average distances.

Surprisingly, some recent studies employing the GGA and GGA+U functionals have reported significantly higher diffusion barriers for the TSH pathway than that observed here, e.g. for $NaCoO_2$ (0.35 eV)[91, 92], Na-NCM-333 (0.29 eV)[92] and Li-NCMs (0.35 for neighboring Ni^{+2}).[33] We note that in the above stated studies the predicted *c* lattice parameters were lower than that of corresponding experimental values. The high Li/Na diffusion barriers in the above stated studies might be due to too low *c* lattice parameters.

In NCM based layered materials in the high lithiation limit, Li migration primarily follows an ODH pathway.[33] Our computed diffusion rate at 300 K, for the ODH pathway (3.6×10^{-11} cm^2/sec) is found to be in good agreement with the experimental Li diffusion coefficient for NCM-523 (e.g. 4.64×10^{-11} cm^2/sec[93] and 1.55×10^{-12} cm^2/sec[30]) in the fully lithiated limit. We find that for TSH pathways the diffusion rates are quite high, as high as 8.6×10^{-5} cm^2/sec. We note that as the first principle calculations are performed on idealized bulk cathode materials at thermodynamic equilibrium, as is usually the case, the current study can only mimic a single, slow C-rate. However, Li diffusion barriers in layered materials strongly depend on Li concentration due to changes in oxidation states of TMs on de-intercalation.[87] Since Li ion vacancies repel each other, it is less likely that structures will contain solely di-vacancies, except at very low lithiation limits. Thus, the net diffusion rate in partially delithiated states likely contains contributions from both TSH and ODH pathways, depending upon availability of di-vacancies near the migrating ion.

Conclusions

In this paper, we present a systematic study of NCM-523 for use in Li-ion batteries. We present a procedure to elucidate the lowest energy cationic ordering using a funneled multi-scale approach. We show that the PBE and PBE+D3 methods reproduce the experimental trends of intercalation potentials better than that of PBE +U, while dispersion corrections (i.e. D3) are essential to correctly describe the change in the *c* cell parameter during Li-intercalation. The formation energies of partially de-intercalated states of NCM-523 suggest solid solution behavior during the de-intercalation cycles. We also show that the Li diffusion rate in NCM-523 is significantly lower than that of $LiCoO_2$ for both ODH and TSH pathway. Our results of Li diffusion are in good agreement with the experimental diffusion coefficients. The results of the electronic structure clearly confirm the active role of Ni in the electrochemical redox process. We also show that Ni oxidizes first, followed by Co, while Mn remains inactive during the lithium ion deintercalation in NCM-523.

Acknowledgements: This work was supported by the Israel Science Foundation (grant No 2797/11) and Israel National Research Center for Electrochemical Propulsion (INREP) consortium.

Supporting Information: Details of the computational and experimental methods, Buckingham potential parameters, lattice and structural parameters obtained by atomistic simulation, electronic structure of NCM-523 obtained using PBE +U and PBE +U+D3 methods and changes in average magnetic moments of TMs of NCM-523 as a function of Li concentration.

References:

1. V. Etacheri, R. Marom, R. Elazari, G. Salitra and D. Aurbach, *Energ Environ Sci*, 2011, **4**, 3243-3262.
2. J. B. Goodenough and Y. Kim, *Chem. Mater.*, 2009, **22**, 587-603.
3. A. Manthiram, *J. Phys. Chem. Lett.*, 2011, **2**, 176-184.
4. M. M. Thackeray, C. Wolverton and E. D. Isaacs, *Energy Environ. Sci.*, 2012, **5**, 7854-7863.
5. G. Ceder, *Mrs Bull*, 2010, **35**, 693-701.
6. M. S. Islam and C. A. Fisher, *Chem. Soc. Rev.*, 2014, **43**, 185-204.
7. K. Mizushima, P. C. Jones, P. J. Wiseman and J. B. Goodenough, *Mater. Res. Bul.*, 1980, **15**, 783-789.
8. J. N. Reimers and J. R. Dahn, *J. Electrochem. Soc.*, 1992, **139**, 2091-2097.
9. Y. Shao-Horn, L. Croguennec, C. Delmas, E. C. Nelson and M. A. O'Keefe, *Nat. Mater.*, 2003, **2**, 464-467.
10. T. Ohzuku and A. Ueda, *J. Electrochem. Soc.*, 1994, **141**, 2972-2977.
11. M. M. Thackeray, S.-H. Kang, C. S. Johnson, J. T. Vaughey, R. Benedek and S. A. Hackney, *J. Mater. Chem.*, 2007, **17**, 3112-3125.
12. A. K. Padhi, K. S. Nanjundaswamy and J. B. Goodenough, *J. Electrochem. Soc.*, 1997, **144**, 1188-1194.
13. K. Amine, H. Yasuda and M. Yamachi, *Electrochem. Solid State Lett.*, 2000, **3**, 178-179.
14. C. Delacourt, L. Laffont, R. Bouchet, C. Wurm, J.-B. Leriche, M. Morcrette, J.-M. Tarascon and C. Masquelier, *J. Electrochem. Soc.*, 2005, **152**, A913-A921.
15. F. Zhou, M. Cococcioni, K. Kang and G. Ceder, *Electrochemistry commun.*, 2004, **6**, 1144-1148.
16. S. K. Martha, J. Grinblat, O. Haik, E. Zinigrad, T. Drezen, J. H. Miners, I. Exnar, A. Kay, B. Markovsky and D. Aurbach, *Angew. Chem. Int. Ed.*, 2009, **48**, 8559-8563.
17. T. Muraliganth and A. Manthiram, *J. Phys. Chem. C*, 2010, **114**, 15530-15540.
18. A. Osnis, M. Kosa, D. Aurbach and D. T. Major, *J. Phys. Chem. C*, 2013, **117**, 17919-17926.
19. T. Ohzuku, A. Ueda and M. Nagayama, *J. Electrochem. Soc.*, 1993, **140**, 1862-1870.
20. A. Yamada, S. C. Chung and K. Hinokuma *J. Electrochem. Soc.*, 2001, **148**, A224-A229.
21. J. Cho, Y. W. Kim, B. Kim, J. G. Lee and B. Park, *Angew. Chem. Int. Ed.*, 2003, **42**, 1618-1621.
22. M. S. Whittingham, *Chem. Rev.*, 2004, **104**, 4271-4302.
23. W. Liu, P. Oh, X. Liu, M.-J. Lee, W. Cho, S. Chae, Y. Kim and J. Cho, *Angew. Chem. Int. Ed.*, 2015, **54**, 4440-4457.
24. J. R. Dahn, U. von Sacken and C. A. Michal, *Solid State Ionics*, 1990, **44**, 87-97.
25. I. Saadoune and C. Delmas, *J. Mater. Chem.*, 1996, **6**, 193-199.
26. E. Rossen, C. D. W. Jones and J. R. Dahn, *Solid State Ionics*, 1992, **57**, 311-318.
27. Z. Lu, D. MacNeil and J. Dahn, *Electrochem. Solid State Lett.*, 2001, **4**, A200-A203.
28. T. Ohzuku and Y. Makimura, *Chem. Lett.*, 2001, **30**, 642-643.
29. M. E. Spahr, P. Novák, B. Schnyder, O. Haas and R. Nesper, *J. Electrochem. Soc.*, 1998, **145**, 1113-1121.

30. W. Hua, J. Zhang, Z. Zheng, W. Liu, X. Peng, X.-D. Guo, B. Zhong, Y.-J. Wang and X. Wang, *Dalton Trans.*, 2014, **43**, 14824-14832.
31. S.-K. Jung, H. Gwon, J. Hong, K.-Y. Park, D.-H. Seo, H. Kim, J. Hyun, W. Yang and K. Kang, *Adv. Energy Mater.*, 2014, **4**.
32. D. Aurbach, O. Srur-Lavi, C. Ghanty, M. Dixit, O. Haik, M. Talianker, Y. Grinblat, N. Leifer, R. Lavi and D. T. Major, *J. Electrochem. Soc.*, 2015, **162**, A1014-A1027.
33. Y. Wei, J. Zheng, S. Cui, X. Song, Y. Su, W. Deng, Z. Wu, X. Wang, W. Wang, M. Rao, Y. Lin, C. Wang, K. Amine and F. Pan, *J. Am. Chem. Soc.*, 2015, **137**, 8364-8367.
34. M. S. Islam, R. A. Davies and J. D. Gale, *Chem. Mater.*, 2003, **15**, 4280-4286.
35. H. Yu, Y. Qian, M. Otani, D. Tang, S. Guo, Y. Zhu and H. Zhou, *Energ. Environ. Sci.*, 2014, **7**, 1068-1078.
36. J.-r. He, Y.-f. Chen, P.-j. Li, Z.-g. Wang, F. Qi and J.-b. Liu, *RSC Advances*, 2014, **4**, 2568-2572.
37. Q. Sa, J. A. Heelan, Y. Lu, D. Apelian and Y. Wang, *ACS Appl. Mater. Interfaces*, 2015, **7**, 20585-20590.
38. Y. Koyama, I. Tanaka, H. Adachi, Y. Makimura and T. Ohzuku, *J. Power Sources*, 2003, **119–121**, 644-648.
39. B. J. Hwang, Y. W. Tsai, D. Carlier and G. Ceder, *Chem. Mater.*, 2003, **15**, 3676-3682.
40. W.-S. Yoon, C. P. Grey, M. Balasubramanian, X.-Q. Yang, D. A. Fischer and J. McBreen, *Electrochem. Solid State Lett.*, 2004, **7**, A53-A55.
41. W.-S. Yoon, M. Balasubramanian, K. Y. Chung, X.-Q. Yang, J. McBreen, C. P. Grey and D. A. Fischer, *J. Am. Chem. Soc.*, 2005, **127**, 17479-17487.
42. D. Zeng, J. Cabana, J. Bréger, W.-S. Yoon and C. P. Grey, *Chem. Mater.*, 2007, **19**, 6277-6289.
43. L. S. Cahill, S. C. Yin, A. Samoson, I. Heinmaa, L. F. Nazar and G. R. Goward, *Chem. Mater.*, 2005, **17**, 6560-6566.
44. Z. Lu, Z. Chen and J. R. Dahn, *Chem. Mater.*, 2003, **15**, 3214-3220.
45. J. D. Gale and A. L. Rohl, *Mol. Simul.*, 2003, **29**, 291-341.
46. G. Kresse and J. Hafner, *Phys. Rev. B*, 1993, **47**, 558-561.
47. G. Kresse and J. Hafner, *Phys. Rev. B*, 1994, **49**, 14251-14269.
48. G. Kresse and J. Furthmüller, *Comp. Mater. Sci.*, 1996, **6**, 15-50.
49. G. Kresse and J. Furthmüller, *Phys. Rev. B*, 1996, **54**, 11169-11186.
50. S. Dudarev, G. Botton, S. Savrasov, C. Humphreys and A. Sutton, *Phys. Rev. B.*, 1998, **57**, 1505.
51. J. P. Perdew, K. Burke and M. Ernzerhof, *Phys. Rev. Lett.*, 1996, **77**, 3865-3868.
52. N. A. Chernova, M. Ma, J. Xiao, M. S. Whittingham, J. Breger and C. P. Grey, *Chem. Mater.*, 2007, **19**, 4682-4693.
53. S. Grimme, J. Antony, S. Ehrlich and H. Krieg, *J. Chem. Phys.*, 2010, **132**, 154104.
54. J. Klimeš, D. R. Bowler and A. Michaelides, *Phys. Rev. B.*, 2011, **83**, 195131.
55. K. Jiří, R. B. David and M. Angelos, *J. Phys. Condens. Matter*, 2010, **22**, 022201.
56. G. Henkelman, B. P. Uberuaga and H. Jónsson, *J. Chem. Phys.*, 2000, **113**, 9901-9904.
57. S. P. Ong, V. L. Chevrier, G. Hautier, A. Jain, C. Moore, S. Kim, X. Ma and G. Ceder, *Energ. Environ. Sci.*, 2011, **4**, 3680-3688.
58. W.-S. Yoon, S. Iannopollo, C. P. Grey, D. Carlier, J. Gorman, J. Reed and G. Ceder, *Electrochem. Solid State Lett.*, 2004, **7**, A167-A171.
59. F. Weill, N. Tran, L. Croguennec and C. Delmas, *J. Power Sources*, 2007, **172**, 893-900.

60. Y. S. Meng, G. Ceder, C. P. Grey, W. S. Yoon, M. Jiang, J. Bréger and Y. Shao-Horn, *Chem. Mater.*, 2005, **17**, 2386-2394.
61. P. Strobel and B. Lambert-Andron, *J. Solid State Chem.*, 1988, **75**, 90-98.
62. H. H. Li, N. Yabuuchi, Y. S. Meng, S. Kumar, J. Breger, C. P. Grey and Y. Shao-Horn, *Chem. Mater.*, 2007, **19**, 2551-2565.
63. J. M. Paulsen and J. R. Dahn, *J. Electrochem. Soc.*, 2000, **147**, 2478-2485.
64. J. Hafner, *J. Comput. Chem.*, 2008, **29**, 2044-2078.
65. G. G. Amatucci, J. M. Tarascon and L. C. Klein, *J. Electrochem. Soc.*, 1996, **143**, 1114-1123.
66. S. C. Yin, Y. H. Rho, I. Swainson and L. F. Nazar, *Chem. Mater.*, 2006, **18**, 1901-1910.
67. S. Laubach, S. Laubach, P. C. Schmidt, D. Ensling, S. Schmid, W. Jaegermann, Thi, K. Nikolowski and H. Ehrenberg, *Phys. Chem. Chem. Phys.*, 2009, **11**, 3278-3289.
68. Y. Koyama, N. Yabuuchi, I. Tanaka, H. Adachi and T. Ohzuku, *J. Electrochem. Soc.*, 2004, **151**, A1545-A1551.
69. J. P. Perdew and S. Kurth, in *A primer in density functional theory*, Springer, 2003, pp. 1-55.
70. M. Aykol, S. Kim and C. Wolverton, *J. Phys. Chem. C*, 2015, **119**, 19053-19058.
71. C. Eames, J. M. Clark, G. Rousse, J.-M. Tarascon and M. S. Islam, *Chem. Mater.*, 2014, **26**, 3672-3678.
72. D. Kim, J.-M. Lim, Y.-G. Lim, J.-S. Yu, M.-S. Park, M. Cho and K. Cho, *Chem. Mater.*, 2015, **27**, 6450-6456.
73. J. Wang, Y. Yu, B. Li, T. Fu, D. Xie, J. Cai and J. Zhao, *Phys. Chem. Chem. Phys.*, 2015, **17**, 32033-32043.
74. A. Van der Ven, M. K. Aydinol, G. Ceder, G. Kresse and J. Hafner, *Phys. Rev. B.*, 1998, **58**, 2975-2987.
75. T. Motohashi, Y. Katsumata, T. Ono, R. Kanno, M. Karppinen and H. Yamauchi, *Chem. Mater.*, 2007, **19**, 5063-5066.
76. S. Kawasaki, T. Motohashi, K. Shimada, T. Ono, R. Kanno, M. Karppinen, H. Yamauchi and G.-q. Zheng, *Phys. Rev. B*, 2009, **79**, 220514.
77. J. Sugiyama, J. H. Brewer, E. J. Ansaldo, B. Hitti, M. Mikami, Y. Mori and T. Sasaki, *Phys. Rev. B*, 2004, **69**, 214423.
78. S. Mazumdar and R. T. Clay, *Phys. Status Solidi B*, 2012, **249**, 995-998.
79. W.-S. Yoon, K.-B. Kim, M.-G. Kim, M.-K. Lee, H.-J. Shin, J.-M. Lee, J.-S. Lee and C.-H. Yo, *J. Phys. Chem. B*, 2002, **106**, 2526-2532.
80. W.-S. Yoon, C. P. Grey, M. Balasubramanian, X.-Q. Yang, D. A. Fischer and J. McBreen, *Electrochemical and solid-state letters*, 2004, **7**, A53-A55.
81. D.-H. Seo, A. Urban and G. Ceder, *arXiv:1507.08768*, 2015.
82. W. R. McKinnon and W. R. McKinnon, *Insertion electrodes I: Atomic and electronic structure of the hosts and their insertion compounds*

Solid state electrochemistry, Cambridge University Press, 1994.

83. M. Aydinol, A. Kohan, G. Ceder, K. Cho and J. Joannopoulos, *Phys. Rev. B*, 1997, **56**, 1354.
84. S. Kawasaki, T. Motohashi, K. Shimada, T. Ono, R. Kanno, M. Karppinen, H. Yamauchi and G.-q. Zheng, *Physical Review B*, 2009, **79**, 220514.
85. V. Singh, M. Kosa, K. Majhi and D. T. Major, *J. Chem. Theory Comput.*, 2015, **11**, 64-72.

86. M. Dixit, H. Engel, R. Eitan, D. Aurbach, M. D. Levi, M. Kosa and D. T. Major, *J. Phys. Chem. C*, 2015, **119**, 15801-15809.
87. A. Van der Ven and G. Ceder, *Electrochem. Solid State Lett.*, 2000, **3**, 301-304.
88. K. Kang and G. Ceder, *Phys. Rev. B.*, 2006, **74**, 094105.
89. K. Kang, Y. S. Meng, J. Bréger, C. P. Grey and G. Ceder, *Science*, 2006, **311**, 977-980.
90. S. Lee and S. S. Park, *J. Phys. Chem. C*, 2012, **116**, 6484-6489.
91. J. Su, Y. Pei, Z. Yang and X. Wang, *Comp. Mater. Sci.*, 2015, **98**, 304-310.
92. J. Su, Y. Pei, Z. Yang and X. Wang, *RSC Adv.*, 2015, **5**, 27229-27234.
93. L. Li, Z. Chen, L. Song, M. Xu, H. Zhu, L. Gong and K. Zhang, *J. Alloy. Comp.*, 2015, **638**, 77-82.

TOC figure

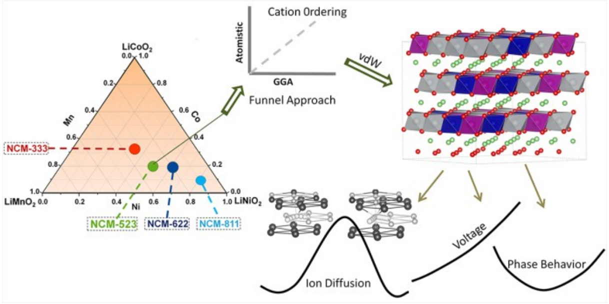

The cation ordering, thermodynamics and diffusion kinetics of $LiNi_{0.5}Co_{0.2}Mn_{0.3}O_2$ (NCM-523) are studied using multi-scale funnel approach with vdW corrections.